Optimization of synthesis a new composite of nano-MgO, CNT and Graphite as a catalyst in heterogeneous catalytic ozonation for the treatment of pesticide-laden wastewater

Ghorban Asgari[a,b], Abdolmotaleb Seidmohammadi[a,b], Javad Faradmal[c,d], Ali Esrafili[e,f], Mohammad Noori Sepehr[g,h], Maghsoud Jafarinia[b,*]

[a] Social Determinants of Health Research Center (SDHRC), Hamadan University of Medical Sciences Hamadan, Iran
[b] Department of Environmental Health Engineering, School of Public Health, Hamadan University of Medical Sciences, Hamadan, Iran
[c] Modeling of Noncommunicable Diseases Research Center, Hamadan University of Medical Sciences, Hamadan, Iran
[d] Department of Biostatistics and Epidemiology, School of Public Health, Hamadan University of Medical Sciences, Hamadan, Iran
[e] Research Center for Environmental Health Technology, Iran University of Medical Sciences, Tehran, Iran
[f] Department of Environmental Health Engineering, School of Public Health, Iran University of Medical Sciences, Tehran, Iran
[g] Research Center for Health, Safety and Environment, Alborz University of Medical Sciences, Karaj, Iran
[h] Department of Environmental Health Engineering, School of Public Health, Alborz University of Medical Sciences, Karaj, Iran

ARTICLE INFO

ABSTRACT

The production of an efficient, reusable, stable and easily separable catalyst in the ozonation process through a reliable procedure is one of the essential requirements of the catalytic ozonation process (COP). In this study, the nano-MgO/CNT/Graphite composite was synthesized to use as a new catalyst in the COP. Synthesis of the nano-MgO/CNT/Graphite was carried out based on the extreme vertices mixture design (EVMD) using three components; MgO nanoparticles, carbon nanotubes (CNTs) and Graphite. Based on EVMD, 9 compositions were produced. For assessing the catalytic activity of synthesized compositions, pesticide manufacturing plant wastewater (PMPW) (initial COD = 617 mg/L and TOC = 121) was treated in COP with new synthesized catalytic. The highest COD and TOC removal and destruction efficiencies were attained with composition C-9. The surface area of the optimum nano-MgO/CNT/Graphite was calculated to be had 221.631 $m^2 g^{-1}$ and a high density of basic surface functional groups. Kinetics of PMPW oxidation indicated that the rate of COD and TOC removal efficiencies in the optimum nano-MgO/CNT/Graphite/O_3 process were 12.73 (13.24/1.04 mg COD/L.min) and 7.11 (1.44/0.2 mg TOC/L.min) times as high as those in the single ozonation (SOP), respectively. Clearly, the optimum nano-MgO/CNT/Graphite showed a significant ability in catalysis of the ozonation process of organic materials by means of increasing O_3 decomposition and ˙OH production. The synthesized optimum nano-MgO/CNT/Graphite was reusable because of the stability and durability of the catalytic activities.

1. Introduction

Recently, advanced oxidation methods (AOPs) such as O_3/H_2O_2 [1], O_3/UV [2], UV/H_2O_2 [3], UV photolysis [3], photocatalytic oxidation with TiO_2 [4,5] have been applied to remove organic substances from aqueous solution. Catalytic ozonation as an effective process has given special attention to the removal of organic matter from aqueous solutions. Catalytic ozonation has to bring about fast removal of organic contaminants and higher efficient mineralization of refractory substances [6,7]. COP would be branched into two subcategory, which accelerate the decomposition of ozone and formation of hydroxyl radicals; Homogeneous and Heterogeneous catalytic ozonation. Heterogeneous catalytic ozonation has shown to have a high removal efficiency of organic contaminants from aqueous media [7–9]. In these processes, catalysts were applied for the acceleration of removal of ozone for generation of hydroxyl radicals. Radicals reactions with pollutant molecules are, in contrary with molecular ozone direct reactions, non-selective and rapid [7,9,10]. These non-selective radicals can oxidize the toxic contaminants for converting to easily biodegradable substances [11]. metal oxides, metals on supports (metal oxides and AC), zeolites modified with AC and metals are the most common applied catalysts in heterogeneous catalytic ozonation [7,11]. Many metal

---

oxides such as Magnesium oxide, Manganese dioxide, Zinc oxide, cerium dioxide, titanium dioxide, aluminum oxides and iron oxides have been applied as catalysts [9,12,13]. Of those the applied catalysts, MgO represented perfect catalytic ability to remove a wide range of contaminants, because of the structural stability, extensive activity, low toxicity and environmental friendliness [14–16]. The homogeneous precipitation technique is an efficient process in MgO synthesis, because of feasibility, availability of pristine substances, cost-effectiveness and excellent performance [17,18]. The use of homogenous ozonation for water purification is not logical due to the need to remove metallic ions from purified water, which is almost ineffective. While, given that the metal ions catalytic activity has been observed at low dosage, their use in treating wastewater containing large quantities of organic matter is also not feasible. The use of a heterogeneous catalytic ozonation method due to its capability of reuse is an advantage, but in many cases, its reuse is limited due to the release of the catalyst compounds into the solution, which increases the cost of the treatment process [14,19]. But the inevitable metal leaching limits their application in terms of green development [20].

From 2004, the application of carbon substances as supports of catalyst has been widely considered in heterogeneous catalytic ozonation. Carbon materials such as fullerenes, graphene and CNTs are used for composites synthesizing [21]. Graphene has sheet like structure consisting sp^2 carbons with high mechanical strength, large surface area (2600 m^2/g) and appreciable charge carrier transportation [21]. Furthermore, in recent years, graphene and their oxide products, as a single atomic layer of graphite, have been applied as either catalysts or catalyst supports in ozonation, which represented the extensive high catalytic ability on organic contaminants removal [19]. Also, graphene has the ability to be applied as interesting reinforcements for composites due to the exceptional mechanical and physical characteristics [19]. Recently, graphene has been applied as an effective reinforcement substance for metal matrix composites [22]. Graphite has been applied in wet air oxidation as a catalyst support, which has more stability than CNTs and activated carbon in ozonation because of its excellent graphitic structure and lower faults [18]. CNTs, carbon xerogel and Activated carbon (AC) have been applied as catalyst supporter in AOPs [13,23–25]. CNTs would have a higher ability to use a supports for catalyst, in comparison with AC in the liquid phase reactions because of the excellent thermal, chemical, electrical and mechanical characteristics. The good performance of CNTs used as a catalyst or catalyst support has been proven in catalytic wet air oxidation [26]. CNTs are also known as applicable substances for several objectives, including environmental clean-up perspectives [27,28]. Regarding carbon substances, CNTs have a high ability to act as efficient catalysts or catalyst supports for helping ozone in organic substances degradation in aqueous solution, similar to the performance of activated carbon [27]. Indeed, regarding the mesoporous structures and high surface areas, CNTs would be appropriate to be applied as a supports in the acceleration of the uniform dispersion of active products and in providing higher active sites for catalytic reactions [27]. Furthermore the addition of nanocarbons, influencing the mechanical properties of the composite [22,29–31]. Although the heterogeneous catalytic ozonation has the advantages such as thorough mineralization of refractory pollutants or production of more biodegradable by-products, easily setting and operation of the system and no need for other chemicals [32], but the leaching of the catalyst components such as metal oxides into the bulk solution and more catalyst consumption is the main limitation of such processes [7,33].

As regards the COP is a new method and understudying process, studying and synthesizing a new, persistent, efficient, easily separable and reusable catalyst is essential. Therefore, the purpose of this research was developing a resistant and highly efficient catalyst with more reusability.

A constrained mixture design covers a smaller space within the mixture-simplex design. The phenomenon happens while extra

limitations in the form of upper and/ or lower constraints are put onto the constituent features [34]. These kinds of mixture designs are mentioned to as EVMD. For this purpose, MgO nanoparticles was synthesized successfully. Then, CNT and graphite were mixed with nano-MgO with proportions obtained from the mixture design. Kaolinite used to bond materials to each other. Kaolinite is used for production of porcelain, brick, tiles, and chamotte. The chemical structure of kaolinite is $Al_2Si_2O_5 (OH)_4$ [35]. The obtained composition was directly transferred to an electrical furnace to strength; the temperature was then increased gradually up to 1350 °C and was kept at this temperature for 2 h. By enhancement of the sintering temperature, the relative density and densification of the composites showed an increasing trend [22]. Noteworthy to say that the sintering temperature has a considerable effect on the densification features, microstructural evolution and properties enhancement of matrix composites [22]. The interaction with oxygen at high temperatures causes improving the oxidation of the materials and negatively affects the sintering process. In order to prevent the oxidation of materials during sintering, argon and hydrogen injection was applied [36]. Finally, the composition was crushed and passed through a 40-30-mesh sieve and then stored in a desiccator for use in the experiments.

2. Materials and methods

2.1. Materials

All applied chemicals were purchased from Merck, Germany. All chemicals were of analytical grade and were used without any extra purification. CNT with a purity greater than 95 % were purchased from the Neutrino Company (Tehran, Iran), Graphite with a mesh of 200-150 purchased from Sinchem (Tehran, Iran), purified kaolinite $(Al_2Si_2)_5(OH)_4$ were obtained from Iran China Clay Industries Co.. All solutions were made with ultra-pure water (with an electrical resistance of 18 μΩ cm at 25 °C). Real wastewater samples were taken from the storage tanks of the pesticide manufacturing plant. COD, TOC and pH of wastewater were 6173.5 ± 712 (mg/L), 1214.1 ± 135.28 (mg/L) and 5.7–6.4 respectively. All samples were stored in the refrigerator for further use.

2.2. Synthesis of nano-MgO

For synthesis of nano-MgO, 5.128 g (0.2 M) magnesium nitrate (MgNO$_3$.6H$_2$O) was mixed in approximately 100 ml of de-ionized water in 1 L beaker. After that, 1.6 g (0.4 M) sodium hydroxide was mixed in 100 ml of de-ionized water. Then was added to the magnesium nitrate solution (which was prepared earlier) drop wise with continuous stirring (30 min). The stirring of the solution was performed during 4 h for the generation of the Mg(OH)$_2$ precipitate. The centrifugation of obtained precipitate was carried out at 3000 rpm for 5 min to obtain the magnesium hydroxide gel. Subsequently, the process of washing was done using methanol and distilled water. Then it was dried at 120 °C during 24 h. Finally, the calcination of obtained material was performed at 450 °C during 2 h and nano-MgO particles were created [37].

2.3. Catalyst preparation

The compatibility of compositions with desired components was obtained based on an EVMD, using three components; Magnesium oxide nanoparticles (nano-MgO) as the main constituent of catalyst with a ratio of 81.5–98%; CNTs with an external diameter of less than 20 nm with a ratio of less than 4.5 % and graphite in the size range of 200-150 meshes ASTM with a ratio of 2–14%. To form the bond between components, kaolinite [38] in the size range of smaller than 50 meshes ASTM was added up to 20 % by weight of the mixture as described in Table 1.

The raw materials in accordance with Table 1 and distilled water as

Table 1
Design of Experiments (DOE) and the mean results of adsorption, removal and destruction efficiencies of different synthesized compositions.

Composition code	nano-MgO (%)	Graphite (%)	CNT (%)	COD			TOC		
				Adsorption (%)	Removal in COP (%)	Destruction efficiency (%)	Adsorption (%)	Removal in COP (%)	Destruction efficiency (%)
C-1	98	2	0	3.08	29.11	89.42	2.56	22.05	88.41
C-2	89.75	8	2.25	4.08	39.25	89.61	3.39	31.57	89.27
C-3	91.625	5	3.375	3.57	36.99	90.35	2.96	29.67	90.01
C-4	93.5	2	4.5	3.02	35.09	91.39	2.51	30.08	91.67
C-5	86	14	0	4.71	45.66	89.68	3.91	36.95	89.42
C-6	93.875	5	1.125	3.52	34.97	89.93	2.92	28.97	89.92
C-7	85.625	11	3.375	4.12	45.00	90.84	3.42	35.40	90.34
C-8	87.875	11	1.125	4.19	45.59	90.81	3.48	37.90	90.82
C-9	81.5	14	4.5	3.94	51.29	92.32	3.27	43.68	92.51

much as needed were poured into a 250 ml Stainless Steel Cup. To create a homogeneous mixture, the contents of the cup were rotated at 150 rpm in a planetary mill for a period of 2 h. After drying the slurry at 120 °C, the resulting compositions were pressurized by a hydraulic press of 20 atm (1 Ton/cm^2) to reach desired densification [31].

In order to stabilize the structure and create a persistent compound, all of the specimens were sintered in an electrically heated furnace under hydrogen and argon-controlled atmosphere with a flow of 200 and 50 mL.min^{-1} respectively, for 2 h at 1350 °C using a heating rate of 5 °C/min. The compositions were grinded to obtain fine granules (40-30 mesh) and were washed 3 times with distilled water, then were dried at 90 °C for 48 h and were stored in a desiccator for use in the further experiments [36].

2.4. Catalytic ozonation experiments and optimum catalyst selection

Based on the EVMD, 9 compositions were synthesized. For assessing the efficiency of catalytic activity of compositions, Experiments were taken on PMPW samples. The tests were done in a Pyrex cylindrical impinger as a reactor with total working volume of 500^{cc}, which carried out in a semi-batch mode. The system consisted of three parts; ozone generation and injection, reactor and an exhaust gas purification. The exhaust gas was further purified with a 2 % KI solution to destruct the effluent ozone (see Fig. 1). Ozone was generated by an ozone generator (ARDA, MOG-5G-H). The ozonation rate was constant at 1 g/h throughout the experiments.

All runs were performed at laboratory temperature of 23 ± 3 °C. Control experiments were carried out with sole ozonation to confirm the catalytic activity of the compositions. All variables were considered constant (pH = 7, initial COD and TOC of 10 times diluted wastewater = 617 and 121 mg/L, respectively, catalyst dosage = 1 g/L and ozonation time = 30 min). The pH of the solution was adjusted using
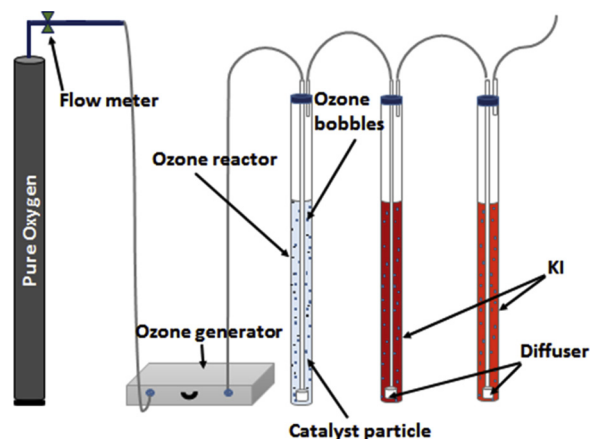

Fig. 1. Schematic diagram of ozonation.

HCl or NaOH normal solutions. The catalyst was easily separated by sedimentation after each run. Before analysis, the residual catalyst was separated through a 0.2 μm PTFE syringe filter. All samples were analyzed for COD and TOC. Besides, adsorption capacity of all compositions was evaluated for quantification of their removal efficiencies.

The spent catalyst (M_c) was separated from the suspension by the sedimentation at the end of the target test and the amounts of adsorbed COD and TOC (M_d) were calculated by measuring the concentrations of COD and TOC after and before the adsorption experiment. Considering the volume of the working solutions (500 mL), the amounts of COD and TOC before (M_b) and after (M_a) the catalytic reaction. Finally, the removal and destruction efficiencies were calculated from below equations.

$$Removal\ efficiency\ (\%) = \left[\frac{(M_b - M_a)}{M_b}\right] \times 100 \tag{1}$$

$$destruction\ efficiency\ (\%) = \left[\frac{(M_b - (M_a + M_d))}{(M_b - M_a)}\right] \times 100 \tag{2}$$

The analyses of the obtained responses were performed using the software Design Expert (version 7.0.0). The possible mathematic models were analyzed using Analysis of variance (one-way ANOVA). The best fitting model was selected for each composition response based on the p-values, F-values and the predictive equations containing only significant terms were built from stepwise multiple regression analysis [39].

The optimum catalyst was selected by using Minitab 17 and Design Expert 7. ANOVA was used to determine the effective level of responses of this model.

The catalytic ozonation mineralization efficacy was evaluated with optimum catalyst. Additionally, for understanding the durability and reusability of the optimum catalyst, the applied catalyst was collected from solution, dried and the catalytic activity was examined for five consecutive cycles.

2.5. Characterization of optimum catalyst

The pore volume and size distribution, specific surface area and morphology, elemental and chemical analysis, structure size, functional groups of surface and pH of point of zero charge (pHpzc) of the synthesized optimum catalyst were studied. The chemical composition of the nano-MgO/CNT/Graphite measured via X-ray diffraction (XRD) (PW1730 – Philips), scanned for 2θ between 10° and 80°. The functional groups on the surface of catalyst were measured by FTIR (Avatar, Thermo) at the wave numbers ranging from 4000 to 400 cm^{-1}. The microstructural evaluation was performed by means of FESEM (FE-SEM, Mira III, Czech Republic) equipped with energy dispersive X-ray (EDX) Microanalysis to characterize the surface structure of the catalyst. The result of EDX Microanalysis was used to show the existence of primary components in the synthesized catalyst. The specific surface

area (SSA) and the pore size measurement of catalyst particles were carried out by the BET using the N_2 adsorption/desorption method at 77 K by using a BELSORP MINI II (Japan) surface area analyzer and calculated according to the Brunauer-Emmett-Teller (BET) and Barrett-Joyner- Hanlenda (BJH) isotherm models. The structure size of catalyst was evaluated by (TEM) with an acceleration voltage of 200 kV (Philips Model CM20). The pHpzc was determined by the conventional method [18].

2.6. Analytical methods

Potassium iodide (KI) technique was applied for measurement of the dosage of ozone [40]. The residual O_3 of the samples was destroyed by adding $Na_2S_2O_3$ to the samples. The standard method of potassium dichromate oxidation was used for measuring COD [40]. A TOC analyzer (Shimadzu, TOC analyzer– VCSH Model) was applied for measuring the TOC of samples. A pH-meter (Sense Ion 37.58, Hack) was applied for measuring the solution pH.

3. Results and discussion

3.1. Comparison of the catalytic activity of various prepared compositions

The COD and TOC degradation efficiencies in the SOP were constant at 9.62 and 7.42 %, respectively. COD and TOC adsorption onto compositions, removal and destruction efficiencies of COD and TOC in COP under the considered conditions were shown in Table 1. According to Table 1, the highest COD and TOC removal efficiencies were attained with composition C-9. This high removal and destruction efficiencies might become from the presence of all each three components of composition in optimum quantity (81.5 % nano-MgO, 14 % graphite and 4.5 % CNT) compared to other compositions.

From these results, it can be concluded that as-prepared composition has a significant synergistic effect in coupling with ozone and effectively enhances the degradation. The better performance of the COP in comparison to the SOP indicated that optimum nano-MgO/CNT/ Graphite possess an excellent catalytic activity in oxidative degradation processes.

3.2. Expert design and validation of model

In this study, the EVMD was applied for determination of the measurement points. This method fully symmetrical distributed experimental points and a well- selected multinomial equation [39]. Performing accurate measurements at every point during the mixture design is expensive, time consuming or simply impractical. Design of Experiments (DOE) is one possible method to address these issues [41]. This approach may be used to optimize experiment plans. The goal is performing the lowest number of experiments while gaining the maximum amount of data for the development of an efficient and reproducible model with the desired properties. To study the significance and the adequacy of the model, Variance analysis (ANOVA) was applied [41]. Analysis of variance results using a set of hierarchical models with increasing complexity using the ANOVA linear model, showed statistical significance (see Tables 2 and 3). According to Table 3 R^2 is 0.9793

and 0.9307 for COD and TOC removal efficiencies respectively, that indicated the model exactly fit the experimentally measured COD and TOC. The significance of each coefficient to the fit of the model was then evaluated by its p-value, which was calculated from the ratio of the coefficient to its standard deviation. According to Table 2 P-value of COD and TOC removal efficiencies are < 0.0001 and 0.0003 respectively, where the coefficients with a p-value less than 0.05 were considered to have a significant influence on the fitting of the model. The Model F-values of 141.79 and 40.31 for COD and TOC removal efficiencies confirmed the model significance and there have been just a 0.01 % and 0.03 % chance that model occurs due to noise. The "Predicted R^2" of 0.9611 and 0.8575 for COD and TOC removal efficiencies are in good agreement with the "Adjusted R^2" of 0.9724 and 0.9077 respectively. The "Adequate Precision" of the model measures the signal to noise ratio. A ratio greater than 4 is suitable. The ratio of 32.371 and 17.991 indicate a sufficient signal. The model would be applied for navigation of the design space. Surface fitting of the tested models is illustrated in Fig. S1.

Table 4 shows the model general analysis, which confirms that it is statistically significant. A comparison of actual with the predicted results revealed a significant correlation of $R^2 = 0.9793$ and 0.9307 in COD and TOC removal efficiencies (Fig. S2A). A normal distribution was obtained by comparing internally studentized residue results to the normal probability values (Fig. S2B). A comparison of internally studentized residues with run number and the predicted data is illustrated in Fig. S3 that confirms the application of the regression model, in which the random distribution trend was not seen.

The main aim of the test was obtaining the obvious information about the component proportions in a mixture marked by the maximum percentage removal efficiency. According to the fit to the model of the linear equation desired for this experiment, the applicability profile for approximating data was produced and subsequently the optimum combination of the catalyst composition was obtained. A predicted composition of the mixture is presented in Table 5. With regard to the desirability and the maximum removal efficiency. The composition C-9 was desired as the optimum catalyst for the next experiments.

3.3. Characteristics of the optimum catalyst

The optimum catalyst was entirely characterized. The XRD diagram of the optimum catalyst is illustrated in Fig. 2. Sharp Peaks observed at $2\theta = 37.17°$, $43.17°$, $62.59°$, $74.93°$ and $78.86°$ associate with MgO. This result matches the major peaks of periclase MgO in the Joint Committee on Powder Diffraction Standards(45-0946) [37]. weak peaks observed at $2\theta = 31.58°$, $36.76°$, $37.17°$, $45°$, $59.65°$, $65.49°$, $69,79°$, and $78.86°$ associate with Al_2MgO_4, $2\theta = 35.9°$, $36.76°$, $37.17°$, $42.05°$, $62.59°$ and $65.49°$ associate with $Al_{0.58}$ $Mg_{0.42}$, $2\theta = 32.48°$, $36.76°$, $37.17°$, $43.17°$, $45°$ and $67.15°$ associate with Al_2O_3, $2\theta = 23.07°$, $25.75°$, $26.71°$, $30°$, $31.58°$, $32.48°$, $35.91°$, $36.76°$, $37.17°$, $39.87°$, $42.05°$, $43.17°$, $45°$, $52.48°$ and $67.15°$ associate with $CaAl_2O_4$. The CNTs and graphite peaks on the XRD did not observed because MgO coated the CNTs and graphite. These results suggest that the MgO as the main constituents of the sintered features had a significant correlation with the features prior synthesizing.

The surface morphologies of the optimum catalyst were

Table 2
Sequential Model Sum of Squares for COD and TOC.

Source	Sum of Squares		df		Mean Square		F Value		p-value Prob > F		
	COD	TOC	COD	TOC	COD	TOC	COD	TOC	COD	TOC	
Linear	384.27	295.20	1	2	192.14	147.60	141.79	40.31	< 0.0001	0.0003	significant
Quadratic	0.25	1.93	2	2	0.13	0.97	0.064	0.19	0.9391	0.8318	
Special cubic	2.18	14.29	2	1	2.18	14.29	1.15	7.46	0.3620	0.719	
Cubic	2.66	2.58	1	1	2.66	2.58	1.75	1.63	0.3164	0.3302	

Table 3
Analysis of variance results for different statistical models.

Source	Std. Dev.		R-Squared		Adjusted R-Squared		Predicted R-Squared		PRESS		
	COD	TOC	COD	TOC	COD	TOC	COD	TOC	COD	TOC	
Linear	1.16	1.91	0.9793	0.9307	0.9724	0.9077	0.9611	0.8575	15.26	45.21	significant
Quadratic	1.40	2.24	0.9799	0.9368	0.9598	0.8737	0.7712	0.1203	89.80	279.02	
Special cubic	1.38	1.38	0.9855	0.9819	0.9613	0.9517	0.6407	0.5390	140.98	146.22	
Cubic	1.23	1.26	0.9923	0.9900	0.9691	0.9600	0.1540	− 0.2237	331.97	388.13	

Table 4
Analysis of variance (ANOVA) for COD and TOC.

Source	Sum of Squares		df		Mean Square		F Value		p-value Prob > F		
	COD	TOC	COD	TOC	COD	TOC	COD	TOC	COD	TOC	
Model	384.27	295.20	2	2	192.14	147.60	141.79	40.31	< 0.0001	0.0003	significant
Residual	8.13	21.97	6	6	1.36	3.66					
Cor Total	392.40	317.17	8	8							

$R^2 = 0.9793, R^2_{Adjusted} = 0.9724, R^2_{Predicted} = 0.9611, AP = 32.371, CV = 2.89$ (for COD).
$R^2 = 0.9307, R^2_{Adjusted} = 0.9077, R^2_{Predicted} = 0.8575, AP = 17.991, CV = 5.81$ (for TOC).

characterized using FESEM (Fig. 3). As seen in Fig. 3, the surface of the optimum catalyst is heterogeneous and porous that has irregular shapes and sizes and MgO keeps its main surface morphology after catalyst synthesizing and were fixed onto each other. These results are in accordance with the results of other researchers [37,42].

Elemental analysis of the catalyst was used EDAX and results are given in Fig. 4. Magnesium (Mg), Carbon (C), aluminum (Al), silica (Si), and oxygen (O) with weight percentages of 27.55 %, 35.04 %, 2.13 %, 2.65 %, and 32.63 %respectively, are the main elements in the optimum catalyst. Figs. 4 and S4 also show that the amounts of aluminum and silica elements that were added by kaolinite to the catalyst as a binding material are negligible and carbon, oxygen and magnesium are the main element in composite. These findings indicate that all elements were effectively bonded with each other in the selected method and MgO successfully coated the CNTs and graphite.

The FTIR spectra of the composite in Fig. 5 shows main peaks at 3430, 2927, 2855, 1735, 1630, 1457, 1171 and $600 \, cm^{-1}$ on the spectra. According to Fig. 5, a strong broad band at $3430 \, cm^{-1}$ can be ascribed to the stretching mode of surface hydroxyl groups (O−H) because of the molecular water physical adsorption [43], whereas the peaks at $1630 \, cm^{-1}$ is corresponding to the C=C terminal double bonds [37] and the peaks at $1735 \, cm^{-1}$ is associated with the C=O stretching vibration of the catalyst [44,45]. The peaks at $2855 \, cm^{-1}$ and $2927 \, cm^{-1}$ illustrate C−H symmetric and antisymmetric stretching vibration, respectively [45]. A wide band at $1457 \, cm^{-1}$ can be assigned to Mg−O stretching mode [18,37]. The peak at $1171 \, cm^{-1}$ is because of the H- ion. A broad peak appeared around $600 \, cm^{-1}$ is associated with Mg−O stretching mode [18,45].

TEM image (Fig. 6) shows that the dispersion of the optimum catalyst particles is relatively high and that there is a broad particle size distribution. The size and shape of the particles are preserved at nano ranges in the different steps of synthesizing and did not obviously destroy the structure of the components.

The N_2 adsorption-desorption isotherms were applied to find the textural features (BET surface area and total pore volume) and the
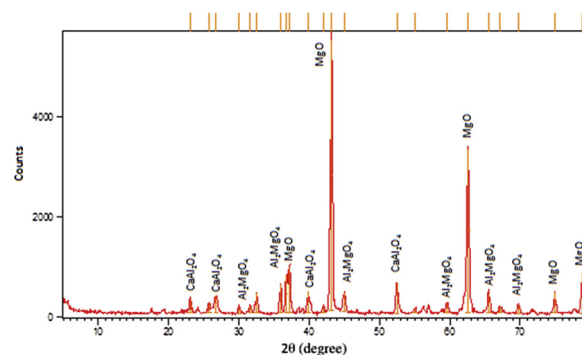

Fig. 2. The XRD pattern of optimum catalyst.

resutls are shown in Fig. 7 and Table 6. As shown, the surface area of optimum catalyst was calculated to be $221.631 \, m^2 \, g^{-1}$. The sample exhibits the mesopore structure with an average pore diameter at 36,582 nm. However, as shown in the SEM image a few agglomerated sites are also visible in the TEM image Which may be related to pressing the composite.

The high catalytic activity of optimum nano-MgO/CNT/Graphite can be justified with the interactions among O_3 molecules and the increased basic functional groups on the high specific surface of optimum catalyst and formation of very reactive species especially ˙OH [7]. In the heterogeneous catalytic ozonation, the basic surface functional groups have a significant effect on increasing the ozone transformation to ˙OH because of the electrophilic features of solution [46,47]. Regarding the chosen pH of aqueous media (7) and PHpzc of the optimum catalyst (9.3) the surface of nano-MgO particles were positively charged in the form of Mg−OH^{2+} in chosen experimental conditions [48]. Furthermore, based on Fig. 5 (FTIR spectra), a high density of hydroxyl groups was present on the catalyst surface. While, ozone has both nucleophilic and electrophilic sites. So, when catalyst was added to the reactor, the dissolved ozone molecules can interact with both the H
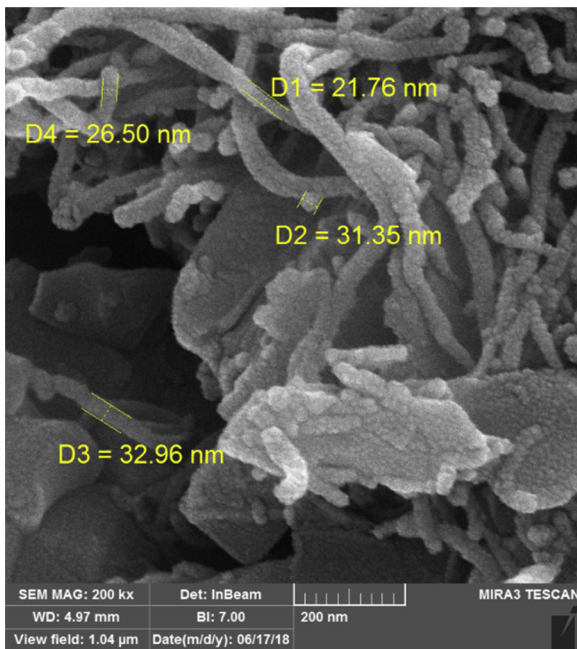
Table 5
Analysis of variance (ANOVA) for COD and TOC and the maximum removal rate.

Number	nano-MgO	Gr	CNT	COD	TOC	Desirability	
1	81.5	14	4.5	51.2058	42.8573	0.979	Selected
2	84.920	11.696	3.384	46.7523	38.7308	0.783	
3	90.253	7.975	1.773	39.769	32.3015	0.477	

Fig. 3. FESEM micrographs of the optimum catalyst.
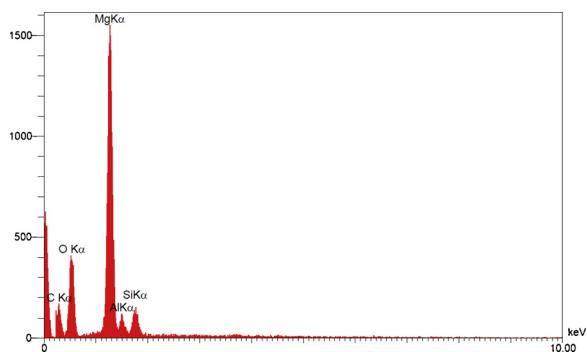
Fig. 4. EDAX analysis of the optimum catalyst.

Fig. 6. TEM image of optimum catalyst.

Fig. 7. Nitrogen adsorption-desorption isotherms of optimum catalyst.

Table 6
Main characteristics of the optimum catalyst.

S_{BET} $(m^2 g^{-1})$	Pore volume $(cm^3 g^{-1})$	Average pore diameter (nm)
221.631	2.9022	36.582

(electrophilic) and O (nucleophilic) atoms of the −OH groups available on the optimum nano-MgO/CNT/Graphite surface. Consequently, the basic functional groups acted as the ozone destruction initiator and accelerated the ·OH formation [49] leading to the COD and TOC removal enhancement. For confirming the enhancement of decomposition of ozone with optimum catalyst, the dosages of O_3 in the inlet and exhaust-gas of the SOP and COP experiments were determined. Apparently, ozone removal in the SOP and COP experiments at the same dosages of O_3, were 21.2 ± 2 and 78 ± 2 %, respectively. So, the
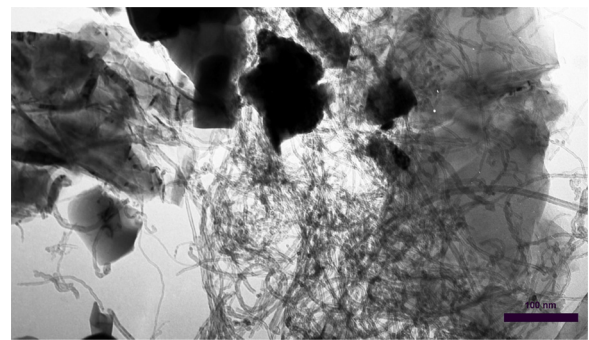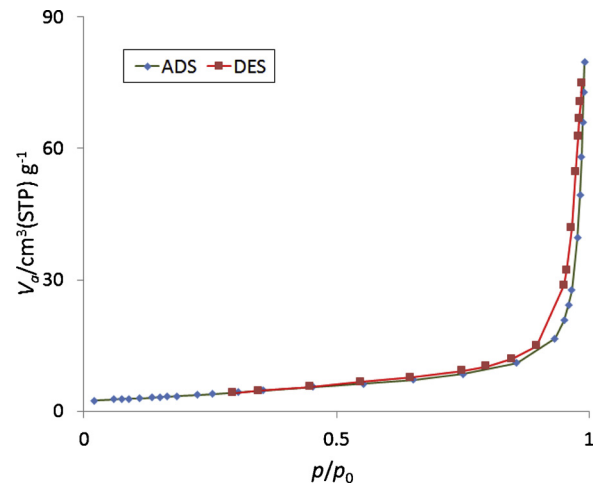
optimum catalyst caused a significant increase in the removal of ozone and ·OH production, which led to increasing the COD and TOC removal percentages. It was deduced that addition of optimum nano-MgO/CNT/Graphite into the ozonation reactor catalyzed the organic materials oxidation by means of increasing the decomposition of ozone and production of oxidative radical species such as ·OH.
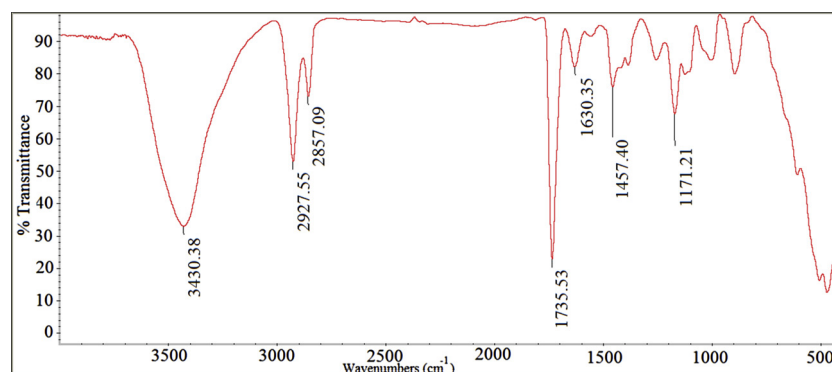

Fig. 5. FTIR spectra of the optimum catalyst.

3.4. Effect of the presence of radical scavengers

To confirm that the organic compounds were oxidized by generated ·OH in COP, COD and TOC removal efficiencies were measured with several common radical scavengers including tert-butanol, sulfate, and carbonate [50]. Fig. S5 shows the COD and TOC removal efficiencies at the pH of 7, catalyst dosage = 1 g/L, initial COD and TOC concentration of 617 and 121 mg/L and run time of 60 min. It is observed that the tert-butanol inhibited the COD and TOC removal. The tert-butanol is a potent radical scavenger with a much higher reaction rate with ·OH species [51,52]. Therefore, the COD and TOC removal efficiencies, decreases in the vicinity of tert-butanol that clearly confirmed the ·OH formation in the COP. Another point observed in Fig. S5 is that the sulfate and carbonate as compared with tert-butanol had less effect on COD and TOC removal efficiencies in the COP. It can be attributed to the point that these anions have a lower reaction rate constant with ·OH and thereby ·OH was mainly scavenged by tert-butanol [52]. Indeed, radical scavengers react with ·OH converting to anion radicals, whereas the oxidation capacity of hydroxyl radicals is much more than anion radicals [53].

3.5. Mineralization of organic compounds in COP and SOP

The average oxidation state of carbon (AOSC) as a most important factor, that describes the nature of wastewater compounds and declares indirectly about the average oxidation state of the organic substances in aqueous media via comparison between TOC and COD using the Eq. (3). [54,55].

$$AOSC = 4 - (4 \times 0.375)\frac{COD}{TOC} \tag{3}$$

where, 0.375 is a ratio between the carbon molecular mass and oxygen to display COD and TOC in mmol.

By description AOSC amounts are ranged between -4 (i.e., methane) and $+4$ (i.e., carbon dioxide), higher AOSC values indicate the better oxidation of the organic materials. However, it should be noted that AOSC does not consider for substances entirely mineralized. It can be seen that in all experiments AOSC increases with time from an initial value around zero as a result of slight degradation of organic substances, however this increment was higher in catalytic experiments [54]. The AOSC value of the starting pesticide wastewater sample was about -1, as the AOSC is low. For sole ozonation, the average oxidation amount of the organic substances increased to 0.2 after 3 h reaction, which however remains low. Adding the optimum catalyst during the ozonation process resulted in a three-step process: from 0 to 30 min (AOSC from -1 to -0.32), from 30 to 60 min (AOSC = $+1.17$) and 1 up to 3 h (AOSC from $+1.17$ to $+3$) (see Fig. S6).

3.6. Catalyst stability and reusability

The catalyst performance, durability and reusability have a significant effect on the catalytic reactions. The durability and reusability studies of optimum nano-MgO/CNT/Graphite were performed in five consecutive ozonation experiments. These findings suggest that prepared optimum nano-MgO/CNT/Graphite could preserve its catalytic property as well as its stability after five consecutive usages and thus it is a reusable catalyst capable of preserving its catalytic activity (see Fig. S7).

3.7. catalytic activity of optimum nano-MgO/CNT/Graphite: kinetic analysis

Different pathways for the COD and TOC removal efficiencies by ozonation with optimum nano-MgO/CNT/Graphite should be taken into account: parent substances or intermediates adsorption onto the catalysts; simple oxidation via O_3 molecules in aqueous media;

oxidation in the aqueous media by free radicals obtained by destruction of ozone initiated by OH^- and HO_2^- ions; Oxidation by free radicals in the aqueous media due to catalytic destruction of O_3; and oxidation on the catalyst surface [56]. With regard to mentioned pathways and obtained findings, the mechanistic approach would be defined as follows: first, the organic substances were degraded via direct ozonation for transformation in intermediates that were more recalcitrant than the parent substances. A group of intermediates can be attached to the surfaces of catalyst. Once ozone begins accumulating in aqueous media, it will lead to reaching the surfaces of catalyst. There, O_3 could be adsorbed onto the surface of catalyst and converting to surface oxide species and releasing free radicals to aqueous media [57]. Meanwhile, ozone has the possibility of reaction with adsorbed compounds. Reactions of surface oxidation and bulk water free radicals had the most effect on the mineralization of the oxidation intermediates.

For a better illustration of the catalytic activity of optimum nano-MgO/CNT/Graphite on the ozonation process, the kinetics of COD and TOC removal efficiencies were compared accordance with the following reaction model (Eqs. (4) and (5)):

$$Ln\left(\frac{C_t}{C_0}\right) = -k_{obs}t \tag{4}$$

$$r_1 = -\frac{dC}{dt} = k_{obs}\,C0 \tag{5}$$

where, C_0 and C_t represent the initial and residual amount of COD and TOC, respectively, and k_{obs} is pseudo-first-order (PFO) reaction rate constant.

According to the obtained findings, the PFO model had a desirable fitness ($R^2 > 0.99$) with both the COD and TOC removal efficiencies. Table 7 shows the findings of the kinetics of COD and TOC removal efficiencies. Accordingly, the rate of COD removal in the COP (r_{COP} = 13.24 mg COD/L.min) was about 12.73 times greater than that in the SOP (r_{SOP} = 1.04 mg COD/L.min). Moreover, the rate of TOC removal in the SOP and COP was 0.2 mg TOC/L.min and 1.44 mg TOC/L.min, respectively. It confirm the significant catalytic activities of the optimum nano-MgO/CNT/Graphite on the ozonation process of COD and TOC removal.

The removal efficiency of optimum nano-MgO/CNT/Graphite was investigated in the COD and TOC removal efficiencies at constant variables (pH = 7, catalyst dosage = 1 g/L). Fig. 8 shows the COD and TOC removal efficiencies in the SOP and O_3/nano-MgO/CNT/Graphite process (COP). The SOP efficacy in the removal of COD and TOC increased from about 1.31%–12.19% and 0.89%–9.56% respectively, with the increase of the reaction time from 5 min to 60 min. According to Fig. 8, addition of optimum nano-MgO/CNT/Graphite into the reactor significantly improved the COD and TOC removal efficiencies. The removal efficiencies of COD and TOC in the COP increased from 5.81 % and 3.18%–72.41% and 51.07 respectively, when the reaction time was increased from 5 to 60 min. Accordingly, the destruction efficiency of optimum nano-MgO/CNT/Graphite on the ozonation process of COD and TOC removal efficiencies enhanced from 80.17%–94.17 % with the reaction time increasing from 5 min to 60 min, indicated that the time did not have negative effect on destruction efficiency and it may be related to low adsorption of organic

Table 7
Kinetic information of COD and TOC removal efficiencies in SOP and COP.

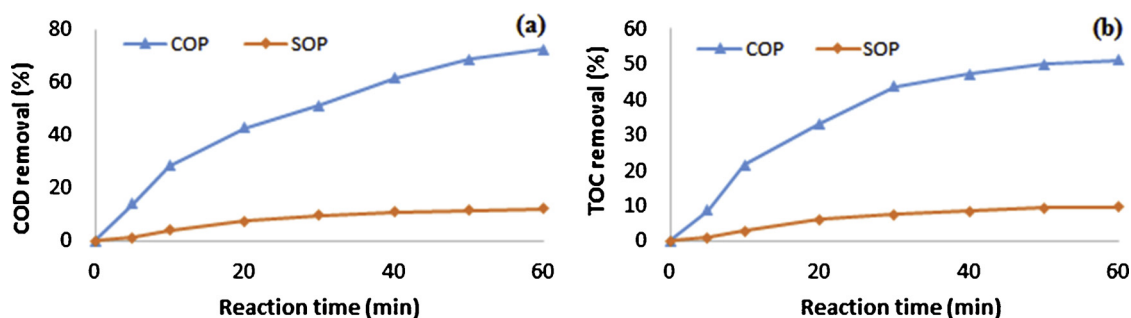|	SOP			COP			$\frac{r_{COP}}{r_{SOP}}$
	R^2	K_{obs} (min^{-1})	r_{SOP} (mg/L.min)	R^2	k_{obs} (min^{-1})	r_{COP} (mg/L.min)	
COD	0.996	0.002	1.04	0.99	0.021	13.24	12.73
TOC	0.994	0.002	0.2	0.991	0.012	1.44	7.11

Fig. 8. Catalytic activity of optimum nano-MgO/CNT/Graphite for (a) COD removal efficiency and (b) TOC removal efficiency of pesticide plant wastewater in the COP as a function of reaction time (Catalyst dosage: 1 g/L, O3 dosage: 1 g O3/h, COD: 617 mg/L, TOC: 185 mg/L pH: 7). The adsorption of COD and TOC onto optimum nano-MgO/CNT/Graphite were < 4.23 % and < 3.64 %, respectively.

materials on catalyst. Fig. S6 illustrates the organic materials mineralization level as a function of contact time. According to the findings, COD and TOC adsorption onto optimum nano-MgO/CNT/Graphite were obtained 4.23 and 3.64 % at the maximum contact time (60 min), respectively. The optimum nano-MgO/CNT/Graphite potential for catalyzing the COD and TOC removal efficiencies in the ozonation reactor was around 56 % during 60 min. Hence, Fig. 8 illustrates that optimum nano-MgO/CNT/Graphite represent significant catalytic activities to degrade and mineralize the organic substances in the ozonation reactor.

4. Conclusions

Magnesium oxide nanoparticles, carbon nanotube and graphite were used to prepare a new catalyst for applying in heterogeneous catalytic ozonation of PMPW. The compatibility of the catalyst with desired components was determined according to an EVMD. Kinetics of PMPW catalytic oxidation showed that the COD and TOC removal efficiencies in the optimum nano-MgO/CNT/Graphite/O$_3$ process were 12.73 (13.24/1.04 mg COD/L.min) and 7.11 (1.44/0.2 mg TOC/L.min) times higher than those in the sole ozonation process (SOP), respectively. Apparently, the optimum nano-MgO/CNT/Graphite showed a significant ability to catalyze the ozonation procedure of organic substances via increasing the decomposition of O$_3$ and production of $^.$OH. The synthesized optimum nano-MgO/CNT/Graphite was proved to be reusable due to its durability of catalytic activity. Ultimately, the developed process is an applicable technique for synthesizing nano-MgO/CNT/Graphite to catalyze the ozonation of organic pollutants in aqueous solution.

Declaration of Competing Interest

There are no conflict of interest.

Appendix A. Supplementary data

Supplementary material related to this article can be found, in the online version, at doi:https://doi.org/10.1016/j.jwpe.2019.101082.

References

[1] E.J. Rosenfeldt, K.G. Linden, S. Canonica, U. von Gunten, Comparison of the efficiency of. OH radical formation during ozonation and the advanced oxidation processes O3/H2O2and UV/H2O2, Water Res. 40 (2006) 3695–3704, https://doi.org/10.1016/j.watres.2006.09.008.

[2] W.K. Lafi, Z. Al-Qodah, Combined advanced oxidation and biological treatment processes for the removal of pesticides from aqueous solutions, J. Hazard. Mater. 137 (2006) 489–497, https://doi.org/10.1016/j.jhazmat.2006.02.027.

[3] X. Kong, J. Jiang, J. Ma, Y. Yang, W. Liu, Y. Liu, Degradation of atrazine by UV/chlorine: efficiency, influencing factors, and products, Water Res. 90 (2016) 15–23, https://doi.org/10.1016/j.watres.2015.11.068.

[4] A.K.R. Police, S.V.P. Vattikuti, K.K. Mandari, M. Chennaiahgari, P.S. Phanikrishna, D.K. Valluri, C. Byon, Bismuth oxide cocatalyst and copper oxide sensitizer in Cu2O/TiO2/Bi2O3 ternary photocatalyst for efficient hydrogen production under solar light irradiation, Ceram. Int. 44 (2018) 11783–11791, https://doi.org/10.1016/j.ceramint.2018.03.262.

[5] P. Wang, P.S. Yap, T.T. Lim, C-N-S tridoped TiO2 for photocatalytic degradation of tetracycline under visible-light irradiation, Appl. Catal. A Gen. 399 (2011) 252–261, https://doi.org/10.1016/j.apcata.2011.04.008.

[6] G. Asgari, J. Faradmal, H.Z. Nasab, H. Ehsani, Catalytic ozonation of industrial textile wastewater using modified C-doped MgO eggshell membrane powder, Adv. Powder Technol. (2019), https://doi.org/10.1016/j.apt.2019.04.003.

[7] J. Nawrocki, B. Kasprzyk-Hordern, The efficiency and mechanisms of catalytic ozonation, Appl. Catal. B Environ. 99 (2010) 27–42, https://doi.org/10.1016/j.apcatb.2010.06.033.

[8] Z. Liu, J. Ma, Y. Cui, B. Zhang, Effect of ozonation pretreatment on the surface properties and catalytic activity of multi-walled carbon nanotube, Appl. Catal. B Environ. 92 (2009) 301–306, https://doi.org/10.1016/j.apcatb.2009.08.007.

[9] B. Kasprzyk-Hordern, M. Ziółek, J. Nawrocki, Catalytic ozonation and methods of enhancing molecular ozone reactions in water treatment, Appl. Catal. B Environ. 46 (2003) 639–669, https://doi.org/10.1016/S0926-3373(03)00326-6.

[10] G. Asgari, A.S. Mohammadi, A. Ebrahimi, Performance of the catalytic ozonation process with pumice in removal of humic acids from aqueous solutions, Int. J. Environ. Health Eng. 1 (2012) 1–7, https://doi.org/10.4103/2277-9183.99327.

[11] H. Zhu, W.W. Ma, H. Han, Y. Han, W.W. Ma, Catalytic ozonation of quinoline using nano-MgO: efficacy, pathways, mechanisms and its application to real biologically pretreated coal gasification wastewater, Chem. Eng. J. 327 (2017) 91–99, https://doi.org/10.1016/j.cej.2017.06.025.

[12] B. Legube, Catalytic ozonation: a promising advanced oxidation technology for water treatment, Catal. Today 53 (1999) 61–72, https://doi.org/10.1016/S0920-5861(99)00103-0.

[13] A. Corma, H. Garcia, A. Leyva, Catalytic activity of palladium supported on single wall carbon nanotubes compared to palladium supported on activated carbon Study of the Heck and Suzuki couplings, aerobic alcohol oxidation and selective hydrogenation, J. Mol. Catal. A: Chem. 230 (2005) 97–105, https://doi.org/10.1016/j.molcata.2004.11.030.

[14] S. Haidari, B. Kamarehie, A. Jafari, M. Birjandi, S. Afrasyabi, Oxalic acid degradation from aqueous solution using ozonation process in the presence of magnesium oxide nanoparticles catalyst stabilized on activated carbon, Int. J. Environ. Health Eng. 5 (2016) 23, https://doi.org/10.4103/2277-9183.196665.

[15] I.W. Siriwardane, R. Udangawa, R.M. de Silva, A.R. Kumarasinghe, R.G. Acres, A. Hettiarachchi, G.A.J. Amaratunga, K.M.N. de Silva, Synthesis and characterization of nano magnesium oxide impregnated granular activated carbon composite for H2S removal applications, Mater. Des. 136 (2017) 127–136, https://doi.org/10.1016/j.matdes.2017.09.034.

[16] G. Moussavi, M. Mahmoudi, Removal of azo and anthraquinone reactive dyes from industrial wastewaters using MgO nanoparticles, J. Hazard. Mater. 168 (2009) 806–812, https://doi.org/10.1016/j.jhazmat.2009.02.097.

[17] G. Moussavi, A. khavanin, R. Alizadeh, The integration of ozonation catalyzed with MgO nanocrystals and the biodegradation for the removal of phenol from saline wastewater, Appl. Catal. B Environ. 97 (2010) 160–167, https://doi.org/10.1016/j.apcatb.2010.03.036.

[18] A. Mashayekh-Salehi, G. Moussavi, K. Yaghmaeian, Preparation, characterization and catalytic activity of a novel mesoporous nanocrystalline MgO nanoparticle for ozonation of acetaminophen as an emerging water contaminant, Chem. Eng. J. 310 (2017) 157–169.

[19] L. Jothinathan, J. Hu, Kinetic evaluation of graphene oxide based heterogenous catalytic ozonation for the removal of ibuprofen, Water Res. 134 (2018) 63–73,

https://doi.org/10.1016/j.watres.2018.01.033.

[20] J. Wang, S. Chen, X. Quan, H. Yu, Fluorine-doped carbon nanotubes as an efficient metal-free catalyst for destruction of organic pollutants in catalytic ozonation, Chemosphere 190 (2018) 135–143, https://doi.org/10.1016/j.chemosphere.2017.09.119.

[21] A.K.R. Police, M. Chennaiahgari, R. Boddula, S.V.P. Vattikuti, K.K. Mandari, B. Chan, Single-step hydrothermal synthesis of wrinkled graphene wrapped TiO2 nanotubes for photocatalytic hydrogen production and supercapacitor applications, Mater. Res. Bull. 98 (2018) 314–321, https://doi.org/10.1016/j.materresbull.2017.10.034.

[22] L.L. Dong, S. Biao, Y. Liu, Y.L. Li, Y.Q. Fu, Y.Q. Zhao, Y.S. Zhang, Sintering effect on microstructural evolution and mechanical properties of spark plasma sintered Ti matrix composites reinforced by reduced graphene oxides, Ceram. Int. 44 (2018) 17835–17844, https://doi.org/10.1016/j.ceramint.2018.06.252.

[23] F.J. Beltrán, J. Rivas, P. Álvarez, R. Montero-de-Espinosa, Kinetics of heterogeneous catalytic ozone decomposition in water on an activated carbon, Ozone Sci. Eng. 24 (2002) 227–237, https://doi.org/10.1080/01919510208901614.

[24] Z.Q. Liu, J. Tu, Q. Wang, Y.H. Cui, L. Zhang, X. Wu, B. Zhang, J. Ma, Catalytic ozonation of diethyl phthalate in aqueous solution using graphite supported zinc oxide, Sep. Purif. Technol. 200 (2018) 51–58, https://doi.org/10.1016/j.seppur.2018.02.025.

[25] Z.Q. Liu, J. Ma, Y.H. Cui, L. Zhao, B.P. Zhang, Influence of different heat treatments on the surface properties and catalytic performance of carbon nanotube in ozonation, Appl. Catal. B Environ. 101 (2010) 74–80, https://doi.org/10.1016/j.apcatb.2010.09.009.

[26] Z.Q. Liu, J. Ma, Y.H. Cui, Carbon nanotube supported platinum catalysts for the ozonation of oxalic acid in aqueous solutions, Carbon N. Y. 46 (2008) 890–897, https://doi.org/10.1016/j.carbon.2008.02.018.

[27] M. Sui, S. Xing, L. Sheng, S. Huang, H. Guo, Heterogeneous catalytic ozonation of ciprofloxacin in water with carbon nanotube supported manganese oxides as catalyst, J. Hazard. Mater. 227–228 (2012) 227–236, https://doi.org/10.1016/j.jhazmat.2012.05.039.

[28] X. Fan, J. Restivo, J.J.M. Órfão, M.F.R. Pereira, A.A. Lapkin, The role of multiwalled carbon nanotubes (MWCNTs) in the catalytic ozonation of atrazine, Chem. Eng. J. 241 (2014) 66–76, https://doi.org/10.1016/j.cej.2013.12.023.

[29] T. Zhu, Y. Li, S. Sang, S. Jin, Y. Li, L. Zhao, X. Liang, Effect of nanocarbon sources on microstructure and mechanical properties of MgO-C refractories, Ceram. Int. 40 (2014) 4333–4340, https://doi.org/10.1016/j.ceramint.2013.08.101.

[30] M. Bag, S. Adak, R. Sarkar, Nano carbon containing MgO-C refractory: effect of graphite content, Ceram. Int. 38 (2012) 4909–4914.

[31] M. Bag, Development of Environment Friendly New Generation MgO-C Brick Using Nano Carbon Development of Environment Friendly New Generation MgO-C Brick Using Nano Carbon, (2011).

[32] C.D. Stan, I. Cretescu, C. Pastravanu, I. Poulios, M. Drăgan, Treatment of pesticides in wastewater by heterogeneous and homogeneous photocatalysis, Int. J. Photoenergy 2012 (2012) 1–7, https://doi.org/10.1155/2012/194823.

[33] Y. Dadban Shahamat, M. Farzadkia, S. Nasseri, A.H. Mahvi, M. Gholami, A. Esrafili, Y.D. Shahamat, M. Farzadkia, S. Nasseri, A.H. Mahvi, M. Gholami, A. Esrafili, Magnetic heterogeneous catalytic ozonation: a new removal method for phenol in industrial wastewater, J. Environ. Heal. Sci. Eng. 12 (2014) 1–12, https://doi.org/10.1186/2052-336X-12-50.

[34] H. Khalilian, A. Semnani, H. Haddadi, M. Nekoeinia, Multiresponse optimization of a hydraulic oil formulation by mixture design and response surface methods, J. Tribol. 138 (2016) 1–5, https://doi.org/10.1115/1.4031397.

[35] G. Varga, The structure of kaolinite and metakaolinite, Epitoanyag 1 (2007) 6–9, https://doi.org/10.14382/epitoanyag-jsbcm.2007.2.

[36] Y. Gui, J.-M. Oh, J.-W. Lim, Sintering properties of Ti-27Nb alloys prepared by using Ti/TiH2 powders under argon and hydrogen sintering processes, Powder Technol. 339 (2018) 775–780, https://doi.org/10.1016/j.powtec.2018.08.022.

[37] G. Moussavi, A.A. Aghapour, K. Yaghmaeian, The degradation and mineralization of catechol using ozonation catalyzed with MgO/GAC composite in a fluidized bed reactor, Chem. Eng. J. 249 (2014) 302–310, https://doi.org/10.1016/j.cej.2014.03.059.

[38] I. Stubna, A. Trnik, F. Chmelik, L. Vozar, Mechanical properties of kaolin-base ceramics during firing, Adv. Ceram. - Charact. Raw Mater. Process. Prop. Degrad. Heal. (2011), https://doi.org/10.5772/19199.

[39] J. Lawson, C. Willden, Mixture experiments in *R* using **mixexp**, J. Stat. Softw. 72 (2016), https://doi.org/10.18637/jss.v072.c02.

[40] APHA/AWWA/WEF, Standard Methods for the Examination of Water and Wastewater, 23rd ed., American Public Health Association, 2015, www.standardmethods.org.

[41] T. Baj, A. Baryluk, E. Sieniawska, Application of mixture design for optimum antioxidant activity of mixtures of essential oils from Ocimum basilicum L., Origanum majorana L. and Rosmarinus officinalis L, Ind. Crops Prod. 115 (2018) 52–61, https://doi.org/10.1016/j.indcrop.2018.02.006.

[42] Q. Zhou, J.W. Yang, Y.Z. Wang, Y.H. Wu, D.Z. Wang, Preparation of nano-MgO/carbon composites from sucrose-assisted synthesis for highly efficient dehydrochlorination process, Mater. Lett. 62 (2008) 1887–1889, https://doi.org/10.1016/j.matlet.2007.10.031.

[43] F.Q. Pires, T. Angelo, J.K.R. Silva, L.C.L. Sá-Barreto, E.M. Lima, G.M. Gelfuso, T. Gratieri, M.S.S. Cunha-Filho, Use of mixture design in drug-excipient compatibility determinations: thymol nanoparticles case study, J. Pharm. Biomed. Anal. 137 (2017) 196–203, https://doi.org/10.1016/j.jpba.2017.01.037.

[44] V.K. Gupta, S. Agarwal, T.A. Saleh, Chromium removal by combining the magnetic properties of iron oxide with adsorption properties of carbon nanotubes, Water Res. 45 (2011) 2207–2212, https://doi.org/10.1016/j.watres.2011.01.012.

[45] S. Gandhi, P. Abiramipriya, N. Pooja, J.J.L. Jeyakumari, A.Y. Arasi, V. Dhanalakshmi, M.R.G. Nair, R. Anbarasan, Synthesis and characterizations of nano sized MgO and its nano composite with poly(vinyl alcohol), J. Non Cryst. Solids 357 (2011) 181–185, https://doi.org/10.1016/j.jnoncrysol.2010.09.050.

[46] R. Andreozzi, V. Caprio, R. Marotta, D. Vogna, Paracetamol oxidation from aqueous solutions by means of ozonation and H2O2/UV system, Water Res. 37 (2003) 993–1004, https://doi.org/10.1016/S0043-1354(02)00460-8.

[47] M. Sánchez-Polo, U. Von Gunten, J. Rivera-Utrilla, Efficiency of activated carbon to transform ozone into ·OH radicals: influence of operational parameters, Water Res. 39 (2005) 3189–3198, https://doi.org/10.1016/j.watres.2005.05.026.

[48] M.E. Labib, The origin of the surface charge on particles suspended in organic liquids, Colloids Surf. 29 (1988) 293–304, https://doi.org/10.1016/0166-6622(88)80124-0.

[49] T. Zhang, C. Li, J. Ma, H. Tian, Z. Qiang, Surface hydroxyl groups of synthetic α-FeOOH in promoting {radical dot}OH generation from aqueous ozone: property and activity relationship, Appl. Catal. B Environ. 82 (2008) 131–137, https://doi.org/10.1016/j.apcatb.2008.01.008.

[50] G. Moussavi, M. Aqanaghad, Performance evaluation of electro-Fenton process for pretreatment and biodegradability improvement of a pesticide manufacturing plant effluent, J. Sustain. Environ. Res. 25 (2015) 249–254.

[51] R. Broséus, S. Vincent, K. Aboulfadl, A. Daneshvar, S. Sauvé, B. Barbeau, M. Prévost, Ozone oxidation of pharmaceuticals, endocrine disruptors and pesticides during drinking water treatment, Water Res. 43 (2009) 4707–4717, https://doi.org/10.1016/j.watres.2009.07.031.

[52] S.J. Jafari, G. Moussavi, H. Hossaini, Degradation and mineralization of diazinon pesticide in UVC and UVC/TiO2 process, Desalin. Water Treat. 57 (2016) 3782–3790, https://doi.org/10.1080/19443994.2014.987171.

[53] A.K. Sharma, R.K. Tiwari, M.S. Gaur, Nanophotocatalytic UV degradation system for organophosphorus pesticides in water samples and analysis by Kubista model, Arab. J. Chem. 9 (2016) S1755–S1764, https://doi.org/10.1016/j.arabjc.2012.04.044.

[54] J. Vittenet, W. Aboussaoud, J. Mendret, J.S. Pic, H. Debellefontaine, N. Lesage, K. Faucher, M.H. Manero, F. Thibault-Starzyk, H. Leclerc, A. Galarneau, S. Brosillon, Catalytic ozonation with γ-Al2O3 to enhance the degradation of refractory organics in water, Appl. Catal. A Gen. 504 (2015) 519–532, https://doi.org/10.1016/j.apcata.2014.10.037.

[55] P. Pocostales, P. Álvarez, F.J. Beltrán, Catalytic ozonation promoted by alumina-based catalysts for the removal of some pharmaceutical compounds from water, Chem. Eng. J. 168 (2011) 1289–1295, https://doi.org/10.1016/j.cej.2011.02.042.

[56] A. Tekle-Röttering, C. von Sonntag, E. Reisz, C. vom Eyser, H.V. Lutze, J. Türk, S. Naumov, W. Schmidt, T.C. Schmidt, Ozonation of anilines: kinetics, stoichiometry, product identification and elucidation of pathways, Water Res. 98 (2016) 147–159, https://doi.org/10.1016/j.watres.2016.04.001.

[57] J.P. Scott, D.F. Ollis, Integration of chemical and biological oxidation processes for water treatment: review and recommendations, Environ. Prog. 14 (1995) 88–103, https://doi.org/10.1002/ep.670140212.